Tissue Imaging Using Nanospray Desorption Electrospray Ionization Mass Spectrometry

Julia Laskin[a], **Brandi S. Heath**[a], **Patrick J. Roach**[a], **Lisa Cazares**[b], and **O. John Semmes**[b]

[a]Chemical and Materials Sciences Division, Pacific Northwest National Laboratory, Richland, W, 99352

[b]Cancer Biology and Infectious Disease Research Center and Department of Microbiology and Molecular Cell Biology, Eastern Virginia Medical School, Norfolk, VA, 23507

Abstract

Ambient ionization imaging mass spectrometry is uniquely suited for detailed spatially-resolved chemical characterization of biological samples in their native environment. However, the spatial resolution attainable using existing approaches is limited by the ion transfer efficiency from the ionization region into the mass spectrometer. Here we present a first study of ambient imaging of biological samples using nanospray desorption ionization (nano-DESI). Nano-DESI is a new ambient pressure ionization technique that uses minute amounts of solvent confined between two capillaries comprising the nano-DESI probe and the solid analyte for controlled desorption of molecules present on the substrate followed by ionization through self-aspirating nanospray. We demonstrate highly sensitive spatially resolved analysis of tissue samples without sample preparation. Our first proof-of-principle experiments indicate the potential of nano-DESI for ambient imaging with a spatial resolution of better than 12 μm. The significant improvement of the spatial resolution offered by nano-DESI imaging combined with high detection efficiency will enable new imaging mass spectrometry applications in clinical diagnostics, drug discovery, molecular biology, and biochemistry.

Keywords

imaging mass spectrometry; nanospray desorption electrospray ionization (nano-DESI); rhodamine; tissue; spatial resolution

Introduction

Molecular imaging using mass spectrometry (MS)[1-4] is rapidly gaining momentum as a powerful technique for chemical characterization of biological materials and real-time identification of tissues in biological and clinical applications.[5-10] Imaging MS is attractive because of its high sensitivity, speed of analysis, and unprecedented chemical specificity that enables simultaneous detection and identification of a broad range of complex molecules in biological samples.[11] Spatially localized sampling in MS is traditionally achieved using secondary ion mass spectrometry (SIMS),[12-17] matrix-assisted laser desorption ionization (MALDI)[1, 5-7, 10] or other laser-based ionization techniques.[5] Despite its success, MALDI imaging requires sample pre-treatment and matrix deposition prior to analysis. In addition, experiments typically are performed in vacuum, which may

Author for correspondence: Julia Laskin, Chemical and Materials Sciences Division, Pacific Northwest National Laboratory, P.O.Box 999 K8-88, Richland, WA 99352 USA, Tel: (509)-371-6136, Fax:(509)-371-6139, Julia.Laskin@pnnl.gov.

affect the spatial distribution of the analyte molecules in the sample. Ambient pressure surface ionization methods have been developed to overcome these limitations.[3, 18-19] Ambient imaging MS of biological tissues with a spatial resolution of 100-500 μm has been performed using desorption electrospray ionization (DESI),[20-22] laser ablation electrospray ionization mass spectrometry (LAESI),[23-24] and infrared laser ablation metastable-induced chemical ionization.[25] Recently, imaging MS with spatial resolution of 20 μm was achieved using matrix-assisted laser ionization in transmission geometry.[26] High spatial resolution (~10 μm) was achieved using scanning microprobe atmospheric pressure MALDI, which enabled the first ambient, MALDI-based histology imaging.[27] However, the application of a matrix was recognized as a principal limitation of this approach. Similar spatial resolution of was reported for tissue imaging using matrix-free nanostructure initiator mass spectrometry (NIMS).[28]

We have developed a nanospray desorption electrospray ionization (nano-DESI) technique[29-30] capable of achieving fast, spatially resolved analysis of complex mixtures of soluble organic and biological molecules on substrates without sample pre-treatment. Similar to DESI[31] and liquid microjunction surface sampling probe (LMJ-SSP),[32] this technique utilizes liquid extraction and ionization of an analyte deposited on a substrate. Here, we demonstrate the first application of nano-DESI to the ambient imaging of biological tissues.

Figure 1a shows schematics of the nano-DESI source; a photograph of the probe taken during one of the tissue-imaging experiments is shown in Figure 1b. Nano-DESI analysis is performed by bringing a liquid bridge formed between two glass capillaries in contact with analyte deposited on a substarate. The primary capillary maintains the solvent flow to the liquid bridge, while the nanospray capillary removes the solvent containing the dissolved analyte from the bridge and generates charged droplets at the mass spectrometer inlet through a self-aspirating nanospray.[29] This geometry provides an important advantage for imaging applications over the coaxial geometry utilized in the LMJ-SSP technique.[32] Specifically, it enables exquisite control of the size of the liquid bridge between the capillaries that can be varied from several milimiters for some applications that require sampling from larger areas on a surface and made smaller than 10 μm for high-resolution imaging experiments. Figure 1c shows a trace on a rhodamine film left by the nano-DESI probe operated in the imaging mode. The width of the white line in the figure representing the sampled area in less than 8 μm indicating the potential of this technique for high-resolution imaging applications. The size of the liquid bridge is determined by the solvent flow rate, as well as the size and relative position of the capillaries. Previously, we showed nano-DESI's ability to sample an analyte from a small area (<100 μm in diameter) on a surface with little or no hysteresis.[29] In this study, we demonstrate that with proper positioning of the capillaries, nano-DESI enables ambient imaging of tissue samples with a spatial resolution better than 12 μm without sample pretreatment.

Experimental Section

Rhodamine grid

Rhodamine grid was imprinted on a plastic surface by gently pressing a red permanent marker against a fine mesh (1000 lpi) placed onto the plastic surface and covered with a piece of printer paper. Figure 2a shows an optical image of the grid sample obtained using this procedure. The average width of the grid lines is 5 μm and the spacing between them is 20 μm. Other preparation approaches did not yield a good-quality grid.

Rat Brain Tissue Sample

The rat brain sample was provided by Dr. Don Smith (PNNL). The brain from a Wistar Hannover male rat, 9 weeks of age, was purchased from Taconic (Hudson, NY). It was sectioned to 10 μm on a cryo-microtome, deposited on an indium-tin oxide coated glass microscope slide and stored at -80°C. The sample was brought to the room temperature prior to analysis.

Human Kidney Tissue Sample

Patients were consented prior to undergoing renal surgery at Sentara Norfolk General Hospital. Study protocols were approved by the institutional review board at Eastern Virginia Medical School. Frozen renal tissues harvested were embedded in OCT freezing media and stored at -80°C. The tissue sample was sectioned at a thickness of 7 μm and mounted on Indium Tin Oxide (ITO) coated slides (Bruker Daltonics Billerica, MA). H&E staining was performed on the adjacent tissue slice using standard procedures. The stained tissues were then scanned with a PathScan Enabler IV (Myer Instruments Houston, TX). The stained tissue was analyzed by a pathologist to determine tissue morphology. The tissue section was identified as papillary renal cell carcinoma Immediately after sectioning, the tissue sections were treated using a standard fixation protocol. Specifically, human tissue sections were washed and fixed with 70% ethanol and 95% ethanol for 30 s each. An additional water wash was performed to remove residual embedding media followed by a repeat of the ethanol washes in 70% and 95%. This procedure preserves the tissue close to its natural state and prevents decay. It should be noted that tissue fixation is not necessary for nano-DESI imaging.

Imaging Mass Spectrometry

Imaging experiments were performed using an LTQ/Orbitrap mass spectrometer (Thermo Electron, Bremen, Germany). Fused Silica capillaries (50 μm ID, 150 μm OD, Polymicro Technologies, L.L.C., Phoenix) were used to create the primary and the nanospray capillaries. The primary capillary was pulled to a final OD of ca. 70 μm. The 10-20 mm long nanospray capillary was mounted in a 1/16″ OD capillary PEEK tubing (Upchruch Scientific, Oak Harbor, USA) and positioned using a Newport manual MS miniature XYZ stage. The relative position of the capillaries was monitored using a Dino-Lite digital microscope (model AM4013ZTL, SunriseDino, Flushing, NY).Tissue samples attached to glass slides were positioned using a high-resolution XYZ stage composed of three MFA series miniature linear stages (Newport, Corporation, Irvine, CA). The stage was controlled using a custom-designed Labview interface developed in our laboratory. All tissue imaging experiments reported in this study were performed under the same experimental conditions. Typical experiment involved scanning of the stage along the X axis at 20 μm/s. The Y coordinate was varied in steps of 100 μm. Mass spectra were acquired in the LTQ in the positive ion mode without any signal averaging. The average acquisition time was 0.25 s/spectrum. The solvent was optimized for the analysis of lipids. A mixture of 7:3:10 (v:v:v) acetonitrile:toluene:methanol was used in these experiments; the typical solvent rate was 2 μL/s. The high solvent flow rate was maintained by inserting the nanospray capillary tip slightly into the heated capillary and by carefully positioning the primary and the nanospray capillaries relative to each other. The high voltage of 2-3 kV was applied to the primary capillary. The heated capillary of the LTQ/Orbitrap instrument was held at 200 °C and biased at 30-50 V.

Typical line scans collected in this study contained ca. 1100 data points. Because data conversion using FireflyTM software (Prosolia Inc.) is limited to 400 data points/scan, we sliced the line scans into three sections. Each section was processed separately and visualized using Biomap (www.msi.maldi.org). For imaging data that could not be

processed using Firefly, line scans for individual *m/z* features were manually exported and visualized using Origin Pro 8.5 (OriginLab Corporation, Northampton, MA).

Results and Discussion

The spatial resolution of imaging mass spectrometry experiments is often defined by the size of the laser spot in laser-based techniques, the size of the ion beam in SIMS and NIMS, or the size of the charged droplet beam in DESI. However, as pointed out by Heeren and co-workers,[33] these characteristics determine the pixel size while the spatial resolution is defined as a minimum distance needed to resolved adjacent features. The spatial resolution can be calibrated using standard calibration substrates. For example, SIMS instruments are often calibrated using a Cu/Al grid. Unfortunately, no calibration standards exist for imaging using soft ionization techniques. In the absence of chemical gradients, imaging resolution can be estimated by examining the distance required for the signal intensity to increase from the baseline to a certain level. For example, Heeren et al. suggested using the distance for which the signal intensity increases from 20% to 80% of the maximum value as a measure of the spatial resolution.[33] In this study, we used imaging of a rhodamine grid deposited on a glass substrate for the initial evaluation of the performance of the nano-DESI imaging.

Imaging of Rhodamine Grid

Imaging of the rhodamine grid was performed by scanning the substrate under the nano-DESI probe at 4 μm/s along the x-axis and step size of 5 μm along the y-axis. Unaveraged spectra were acquired in the positive mode at a rate of 4 spectra/s corresponding to a spectrum per 1 μm. The optical image of a 2×2 section of the grid examined in this experiment (total image size 50 μm × 50 μm) is shown in Figure 2b. The corresponding ion image obtained for the most abundant ion at *m/z* 354 is shown in Figure 2c. The ion signal clearly shows the lines and the gaps between them. Two adjacent line scans obtained by analyzing the grid are shown in Figure 2d. The average line width and the distance between the lines determined from the line scans are 10 ± 3 μm and 17 ± 3 μm, respectively; the average rise time of the signal is 6 ± 2 μm, the fall time is 9 ± 3 μm. Some trailing of the signal observed on the right hand side of the peaks in the line scan most likely originates from small carryover of the analyte. It should be emphasized that because the solvent is propelled fairly quickly, at 2 μL/s, through the nanospray capillary, diffusion of the analyte in the capillary can be safely ignored. Imaging of the rhodamine grid demonstrates high spatial resolution of the nano-DESI imaging experiments. The estimated resolution of 10 μm obtained in this study is comparable to the best spatial resolution obtained using laser-based ambient imaging techniques.[27-28] Notably, it is four times better than the best spatial resolution of 40 μm reported in DESI imaging[34] and more than an order of magnitude better than the spatial resolution obtained using the related liquid extraction, LMJ-SSP, approach.[35]

Imaging of the rhodamine grid also demonstrates that the area sampled by the nano-DESI probe is symmetric. For imaging experiments, the probe is operated in the regime in which the nanospray capillary rapidly removes the solvent supplied by the primary capillary such that the liquid bridge formed between the two capillaries cannot be seen even with the 100× magnification of the camera that visualizes the interaction region. It is reasonable to assume that when the sample is positioned close to the surface, the liquid forms a meniscus that touches the surface thereby removing soluble analyte molecules from the surface and delivering them to the mass spectrometer inlet. Because no external force is applied to the interaction region, this meniscus is most likely symmetric, which is consistent with the symmetry observed in the image of the rhodamine grid. It should be noted that neither the meniscus nor a liquid trail can be seen on the surface during the imaging experiments. In the

next sections we describe first proof-of-principle experiments showing the utility of nano-DESI imaging for the analysis of tissue samples.

Imaging of Rat Brain Tissue

Mass spectrometry has been extensively used for identification, profiling, and imaging of lipids in tissue samples.[36] Lipids are important signalling molecules involved in physiological processes. Abnormal lipid concentrations and localization are correlated with a large number of diseases. Detailed understanding of disease-related changes in lipid distributions in tissues combined with proteomic and genomic data will enable major breakthroughs in biomedical research related to diagnostics and disease prevention. The solvent used in nano-DESI imaging experiments described in this study was optimized for the analysis of lipids. Figure 3a shows a typical single-point, unaveraged mass spectrum obtained from a rat brain tissue sample representing signal in an individual pixel. The observed features are consistent with previously published data.[36] The spectrum is dominated phosphatidylcholines (PC) that were assigned based on the comparison with the literature data reported for similar samples and on the results of MS/MS experiments.[37] Selected MS/MS spectra are shown in Figure S1 of the supporting information. Abundant losses of 59 (trimethylamine) and 183 (PC headgroup) are characteristic of alkali adducts of PC.[36-40] A high signal-to-noise ratio of ~100 was obtained for the largest peak (m/z 782.6) corresponding to a PC 36:4.[36] The spectrum contains an abundant peak corresponding to the $[M-H_2O+H]^+$ ion of cholesterol (m/z 369.3), a broad distribution of phospholipids (m/z 700-900), multiply charged ions in the m/z 1100-1300 and singly charged species in the m/z 1400-1600 range. Similar features were observed in MALDI, DESI and LAESI studies of rat brain tissue samples.[24, 36-37, 39-41]

Imaging experiments were performed by scanning the nano-DESI probe over a relatively small section (4.5 mm × 1.5 mm) of the brain tissue sample with 5 μm pixel size in the x-dimension and 100 μm step size in the y-dimension. It should be noted that precise control of the position of the nano-DESI probe is critical for high-resolution imaging experiments. For example, the probe must be positioned ca. 10 μm above the sample for imaging with better than 10 μm spatial resolution. In this study the distance between the probe and the sample was controlled manually. We are currently developing a second generaiton nano-DESI imaging platform that will enable precise control of the position of the probe for automated high-resolution imaging experiments.

Tissue imaging experiments were performed in a mode, in which the surface was undersampled in the y-dimension to enable analysis of the selected sample area. As a result, the pixel used for image reconstruction is elongated and has a size of 5 μm × 100 μm. However, based on the results of the rhodamine grid imaging experiment described earlier, we believe that the area sampled by the nano-DESI probe in each pixel is symmetric and has a size of ca. 10 μm × 10 μm. It follows that the imaging resolution of nano-DESI defined as the minimum distance necessary to distinguish adjacent features is the same in the x- and y-dimensions and can be estimated from the line scans in the x-dimension.

An optical image of the tissue section and representative ion images are shown in Figure 3b-e. The tissue section is dominated by the grey matter with a small ca. 500 μm inclusion of white matter. Peaks observed in the nano-DESI spectra were divided into three distinct groups according to their spatial profiles: 1) peaks distributed evenly throughout the sample (Figure 3c), 2) peaks showing higher signal in the white matter (Figure 3d), and 3) peaks that decreased in the white matter (Figure 3e). Representative line profiles for different groups of peaks are shown in figure 4. It should be noted that the data shown in Figures 3a and 4 represent the raw signal obtained from the instrument; no normalization or smoothing was used in data processing. Ion images shown in Figures 3b-e were created using the

Biomap software that interpolates between the points. Because of the undersampling in the y-dimension, the images look "streaky". However, based on the imaging of the rhodamine grid described earlier, we believe that there is no sample transport along the y-axis and the "streaks" originate from the image reconstruction. Line profiles demonstrate signal stability across the sample. The observed variation in the signal is attributed to several factors including the variation of lipid concentration in the sample, the stability of the nanospray, and the variation in the distance between the sample and the probe.

The observed increase and decrease of the lipid signal in the white matter is consistent with previously published data.[36] For example, Woods and co-workers showed through MALDI profiling suppression of PC 32:0 (*m/z* 734.6) and enhancement of PC 36:1 (*m/z* 810.6) in the white matter of a rat brain. Similarly, we observed the corresponding decrease of the PC 32:0 signal and increase of the PC 36:1 signal in the white matter. The line scans (Figure 4) show relatively slow gradual increase and descrease in the lipids signal in the white matter region of the tissue. The slow increase in the ion signal could result from a significant chemical gradient on the boundary between the two tissue sections. As a result, the spatial resolution cannot be determined based on the data presented in Figure 4.

In another experiment we performed imaging of a much more heterogeneous human kidney tissue sample under the same experimental conditions. This experiment demonstrated the potential of nano-DESI imaging for detailed analysis of small features present in tissue samples. Figure 5a shows an average nano-DESI spectrum obtained for the 4.5 mm × 2.5 mm kidney tissue sample. The spectrum is dominated by the peak corresponding to water loss from cholesterol ($[M-H_2O+H]^+$, *m/z* 369.3) and cholesteryl ester (*m/z* 413.3). In addition, the spectrum contains a broad distribution of peaks in the *m/z* 530-1000 range and a number of features in the *m/z* 1200-1400 range. Based on tandem MS/MS experiments shown in Figure S2 and high-resolution MS data, the most abundant peaks in the spectrum were assigned to cholesteryl esters cationized on sodium and potassium. For example, the peak at *m/z* 673.5 most likely corresponds to the $[M+Na]^+$ ion of cholesteryl oleate, while peaks at *m/z* 687.5 and 689.5 correspond to $[M+K]^+$ ions of cholesteryl linoleate and cholesteryl oleate, respectively. Similarly, peaks in the the *m/z* 1200-1400 range were attributed to larger cholesteryl esters based on the characteristic loss of 368 observed in the MS/MS spectra.[42] The observation of abundant cholesteryl esters in these imaging experiments is consistent with high concentrations of intracellular cholesteryl esters reported for RCC kidney tissues.[43]

Representative line profiles across the kidney tissue sample are shown in Figures 5b,c. Several groups of peaks were identified in nano-DESI spectra based on their spatial distribution. Peaks originating from the solvent were present in the spectrum both when the probe was placed on the tissue sample and on the glass slide (data not shown). All sample-related peaks (Figure 5b,c) showed significant variation as a function of the probe's position on the sample and vanished immediately once the probe was moved to the glass slide. An optical image of the corresponding region is shown in Figure 5 for comparison. The observed variation in the ion signal is clearly correlated with the features observed in the optical image. For example, a significant increase in the ion signal was observed when the probe was scanned over the small features highlighted with red arrows in Figure 5. However, it is also clear that not all cholesteryl esters are co-localized. Although the general trends in the line profiles of individual peaks are quite similar, obvious differences are seen in the spatial distribution of different peaks. Figure S3 shows several examples of peaks co-localized on the tissue and peaks showing reduced correlation in their spatial distribution. Figure 6 shows a 2-dimensional image for two characteristic cholesteryl esters representing the two major groups of peaks for a 1.2 × 0.6 mm section of the tissue. The optical image and ion images plotted as contour plots further demonstrate further demonstrate the

heterogeneity of the tissue sample with significant variations in the chemical composition on the scale of tens of micrometers that can be examined using high spatial resolution nano-DESI imaging.

Different rates of signal increase and decrease in the line scan features (Figure 5c,d) indicate the presence of chemical gradients on the boundaries between different sections of the tissue sample. Figures 5d,e show an expanded view of two characteristic sharp features observed in the line scans. The upper limit of spatial resolution, 12 μm, in the nano-DESI imaging experiments was estimated based on the rise or decay time of several sharp features as suggested by Heeren and co-workers.[33] This value is in good agreement with the spatial resolution determined by imaging of the rhodamine grid described earlier. It should be noted that the 100-μm spacing between the rows used for recording a two-dimensional image in these first proof-of-principle experiments does not afford determination of the spatial resolution in the second dimension. However, based on the imaging of the rhodamine grid we believe that the spatial resolution of nano-DESI imaging is the same in both x- and y-dimension. We also note that because images of both tissue samples were obtained under the same experimental conditions, the spatial resolution is the same for the rat brain and the human kidney tissue samples. To obtain nano-DESI images wth high spatial resolution in both dimensions, the spacing between the lines must be reduced. However, because in this first study the distance between the probe and the sample was controlled manually and because of the limitations of the existing data analysis tools available to us, acquisition of an image with small spacing between the line scans was not practical. Future studies will address the current limitations of the imaging platform and of the analysis software.

Conclusions

The first application of nano-DESI for imaging MS demonstrates spatially-resolved analysis of tissue samples in ambient environment with a spatial resolution of better than 12 μm and high signal-to-noise ratio in each individual pixel. Although, in this study, we focused on characterization of lipids, future imaging experiments will involve the interrogation of multiple classes of molecules in tissue samples. This can be done either by optimizing the solvent composition for selective analysis of different classes of molecules using nano-DESI or combining nano-DESI with classical MALDI imaging for the complementary spatial analysis of metabolites, lipids, peptides, and proteins. The advantage of nano-DESI imaging is that no sample pre-treatment is necessary prior to analysis for obtaining high-quality ion images. Furthermore, it can be readily implemented on any commercial or custom-designed mass spectrometer. Although the results reported in this study were obtained using unit mass resolution, coupling nano-DESI imaging with high-resolution mass analysis is straightforward. Nano-DESI imaging opens up new opportunities for detailed spatial profiling of biological samples without any sample pretreatment. These capabilities are of interest to applications in drug discovery, clinical diagnostics, molecular biology, and biochemistry.

Supplementary Material

Refer to Web version on PubMed Central for supplementary material.

Acknowledgments

References

1. McDonnell LA, Heeren RMA. Mass Spectrom Rev. 2007; 26:606–643. [PubMed: 17471576]

2. Pol J, Strohalm M, Havlicek V, Volny M. Histochem Cell Biol. 2010; 134:423–443. [PubMed: 20981554]

3. Dill AL, Eberlin LS, Ifa DR, Cooks RG. Chem Commun. 2011; 47:2741–2746.

4. Vickerman JC. Analyst. 2011; 136:2199–2217. [PubMed: 21461433]

5. Cornett DS, Reyzer ML, Chaurand P, Caprioli RM. Nature Methods. 2007; 4:828–833. [PubMed: 17901873]

6. Walch A, Rauser S, Deininger SO, Hofler H. Histochem Cell Biol. 2008; 130:421–434. [PubMed: 18618129]

7. Esquenazi E, Yang YL, Watrous J, Gerwick WH, Dorrestein PC. Natural Product Reports. 2009; 26:1521–1534. [PubMed: 19936384]

8. Cazares LH, Troyer D, Mendrinos S, Lance RA, Nyalwidhe JO, Beydoun HA, Clements MA, Drake RR, Semmes OJ. Clinical Cancer Research. 2009; 15:5541–5551. [PubMed: 19690195]

9. Schafer KC, Szaniszlo T, Gunther S, Balog J, Denes J, Keseru M, Dezso B, Toth M, Spengler B, Takats Z. Anal Chem. 2011; 83:1632–1640.

10. Seeley EH, Caprioli RM. Trends Biotechnol. 2011; 29:136–143. [PubMed: 21292337]

11. Schwamborn K, Caprioli RM. Nature Reviews Cancer. 2010; 10:639–646.

12. Pacholski ML, Winograd N. Chem Rev. 1999; 99:2977. [PubMed: 11749508]

13. McDonnell LA, Piersma SR, Altelaar AFM, Mize TH, Luxembourg SL, Verhaert P, van Minnen J, Heeren RMA. J Mass Spectrom. 2005; 40:160–168. [PubMed: 15706616]

14. Heeren RMA, McDonnell LA, Amstalden E, Luxembourg SL, Altelaar AFM, Piersma SR. Appl Surf Sci. 2006; 252:6827–6835.

15. Chughtai K, Heeren RMA. Chem Rev. 2010; 110:3237–3277. [PubMed: 20423155]

16. Winograd, N.; Garrison, BJ. Annual Review of Physical Chemistry, Vol 61. Leone, SR.; Cremer, PS.; Groves, JT.; Johnson, MA.; Richmond, G., editors. Vol. 61. 2010. p. 305-322.

17. Fletcher JS, Vickerman JC. Anal Bioanal Chem. 2010; 396:85–104. [PubMed: 19669735]

18. Wiseman JM, Puolitaival SM, Takats Z, Cooks RG, Caprioli RM. Angew Chem Int Ed. 2005; 44:7094–7097.

19. Harris GA, Galhena AS, Fernández FM. Anal Chem. 2011; 83:4508–4538. [PubMed: 21495690]

20. Wiseman JM, Ifa DR, Song QY, Cooks RG. Angew Chem Int Ed. 2006; 45:7188–7192.

21. Eberlin LS, Ifa DR, Wu C, Cooks RG. Angew Chem Int Ed. 2010; 49:873–876.

22. Wiseman JM, Ifa DR, Zhu YX, Kissinger CB, Manicke NE, Kissinger PT, Cooks RG. Proc Natl Acad Sci U S A. 2008; 105:18120–18125. [PubMed: 18697929]

23. Nemes P, Vertes A. Anal Chem. 2007; 79:8098–8106. [PubMed: 17900146]

24. Shrestha B, Nemes P, Nazarian J, Hathout Y, Hoffman EP, Vertes A. Analyst. 2010; 135:751–758. [PubMed: 20349540]

25. Galhena AS, Harris GA, Nyadong L, Murray KK, Fernandez FM. Anal Chem. 2010; 82:2178–2181. [PubMed: 20155978]

26. Richards AL, Lietz CB, Wager-Miller JB, Mackie K, Trimpin S. Rapid Commun Mass Spectrom. 2011; 25:815–820. [PubMed: 21337644]

27. Rompp A, Guenther S, Schober Y, Schulz O, Takats Z, Kummer W, Spengler B. Angew Chem Int Ed. 2010; 49:3834–3838.

28. Yanes O, Woo HK, Northen TR, Oppenheimer SR, Shriver L, Apon J, Estrada MN, Potchoiba MJ, Steenwyk R, Manchester M, Siuzdak G. Anal Chem. 2009; 81:2969–2975. [PubMed: 19301920]

29. Roach PJ, Laskin J, Laskin A. Analyst. 2010; 135:2233–2236. [PubMed: 20593081]

30. Roach PJ, Laskin J, Laskin A. Anal Chem. 2010; 82:7979–7986. [PubMed: 20666445]

31. Takats Z, Wiseman JM, Gologan B, Cooks RG. Science. 2004; 306:471–473. [PubMed: 15486296]

32. Van Berkel GJ, Sanchez AD, Quirke JME. Anal Chem. 2002; 74:6216–6223. [PubMed: 12510741]

33. Luxembourg SL, Mize TH, McDonnell LA, Heeren RMA. Anal Chem. 2004; 76:5339–5344. [PubMed: 15362890]

34. Kertesz V, Van Berkel GJ. Rapid Commun Mass Spectrom. 2008; 22:2639–2644. [PubMed: 18666197]

35. Kertesz V, Ford MJ, Van Berkel GJ. Anal Chem. 2005; 77:7183–7189. [PubMed: 16285664]

36. Jackson SN, Wang HYJ, Woods AS. Anal Chem. 2005; 77:4523–4527. [PubMed: 16013869]

37. Manicke NE, Wiseman JM, Ifa DR, Cooks RG. J Am Soc Mass Spectrom. 2008; 19:531–543. [PubMed: 18258448]

38. Harvey DJ. J Mass Spectrom. 1995; 30:1333–1346.

39. Jackson SN, Wang HYJ, Woods AS. J Am Soc Mass Spectrom. 2005; 16:2052–2056. [PubMed: 16253515]

40. Sugiura Y, Setou M. Rapid Commun Mass Spectrom. 2009; 23:3269–3278. [PubMed: 19760647]

41. Nemes P, Woods AS, Vertes A. Anal Chem. 2010; 82:982–988. [PubMed: 20050678]

42. Talbot HM, Head RN, Harris RP, Maxwell JR. Org Geochem. 1999; 30:1403–1410.

43. Gebhard RL, Clayman RV, Prigge WF, Figenshau R, Staley NA, Reesey C, Bear A. J Lipid Res. 1987; 28:1177–1184. [PubMed: 3681141]

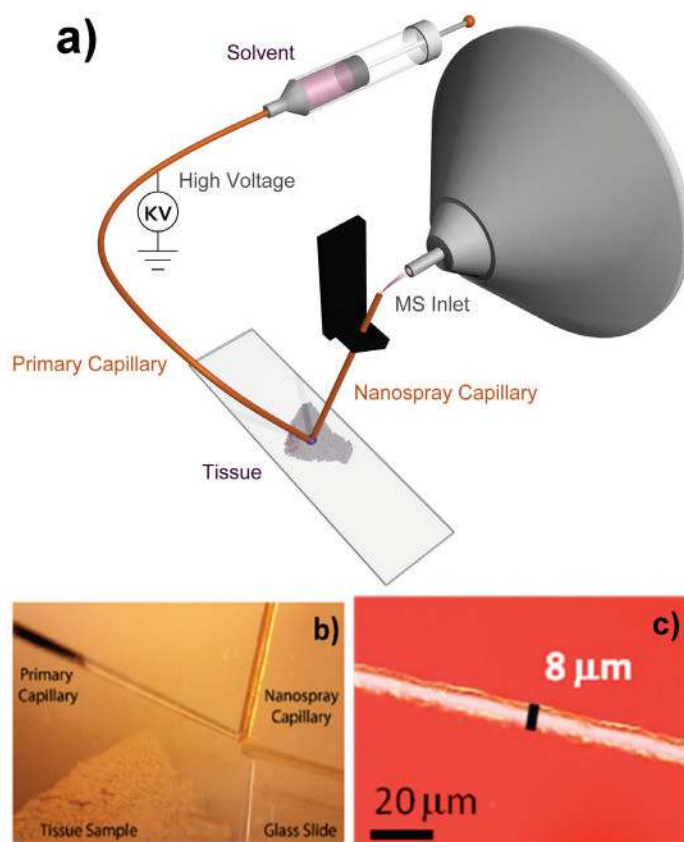**Figure 1.**
a) Schematic drawing of the nanoDESI ion source and b) photograph of the nanoDESI probe taken during ambient imaging of a tissue sample on a glass slide (note that the liquid bridge is not visible to the eye); c) optical image of a trace left by the nanoDESI probe on a rhodamine film on glass.
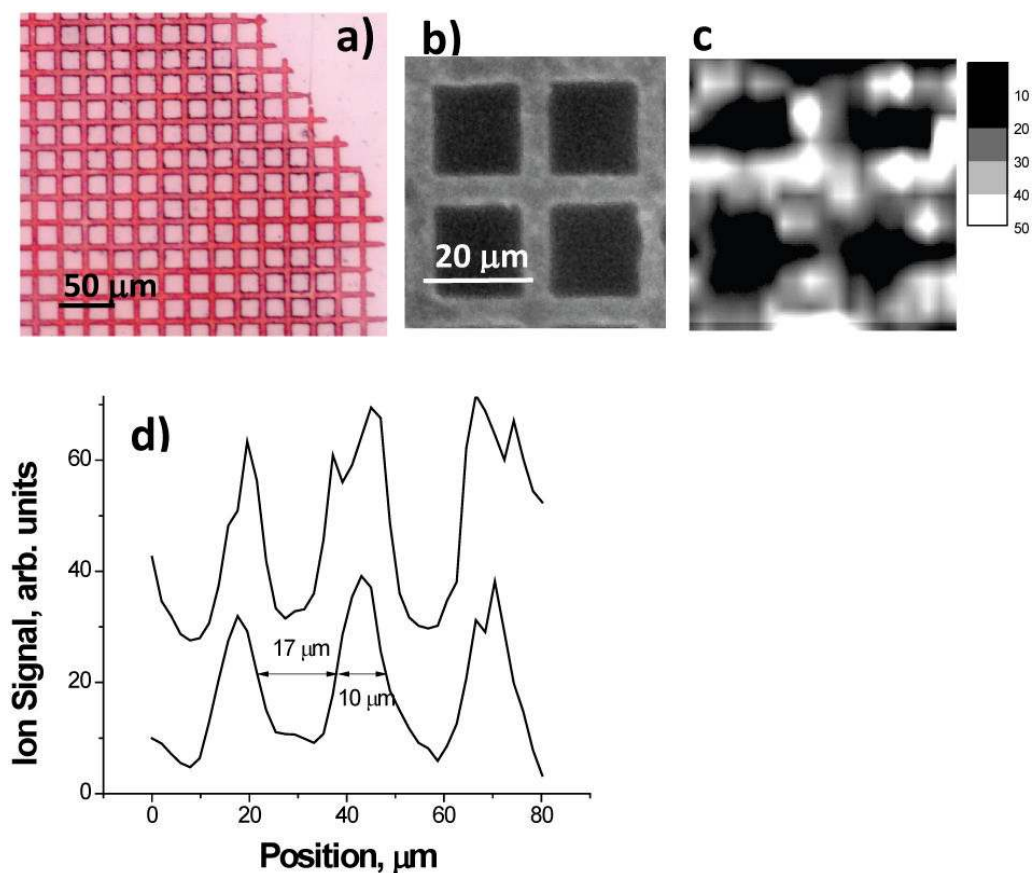
Figure 2.
a) optical image of a rhodamine grid imprinted onto a plastic surface; b) inverted optical image of a 2×2 portion of the grid used for imaging; c) ion image of the 2×2 portion of the grid; d) two adjacent line scans showing the increase and decrease in the ion signal as the nanoDESI probe moves on and off the printed lines. Acquisition parameters: 1 spectrum per 1 μm in the x-dimension, 5 μm step in the y-dimension. Scale bar = 20 μm.
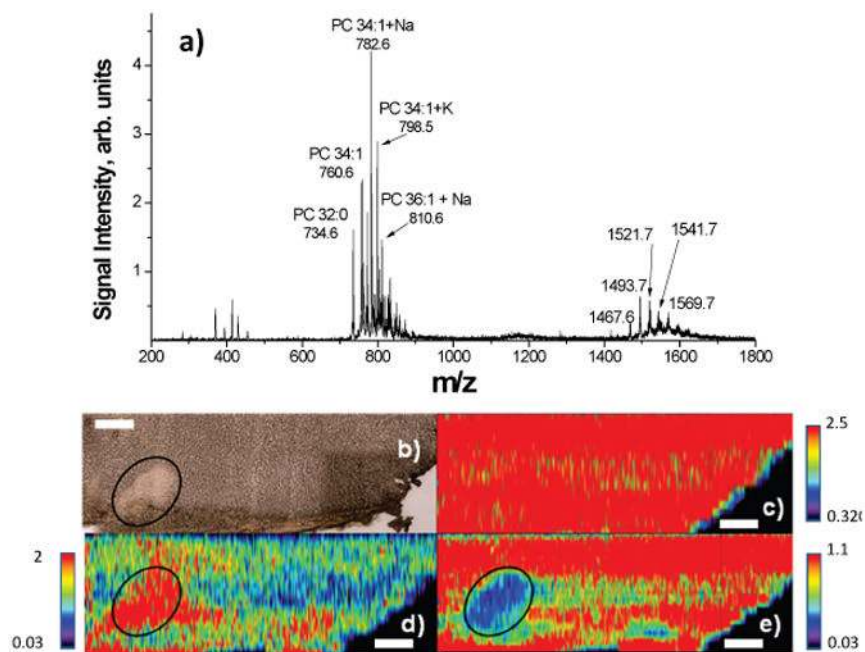
Figure 3.
NanoDESI imaging of a 4.5 mm × 1.5 mm area of the rat brain tissue sample: a) single-scan positive mode nanoDESI spectrum representing signal in one pixel of an image; b) optical image of the rat brain tissue section and representative ion images of peaks, for which signal intensities are c) evenly distributed throughout the tissue sample (*m/z* 782.6), d) increased in the white matter (*m/z* 810.6), and e) decreased in the white matter (*m/z* 734.6). Acquisition parameters: 1100 spectra per line in the x-dimension (1 spectrum per 4.1 μm), 100 μm step in the y-dimension. Scale bar = 500 μm.
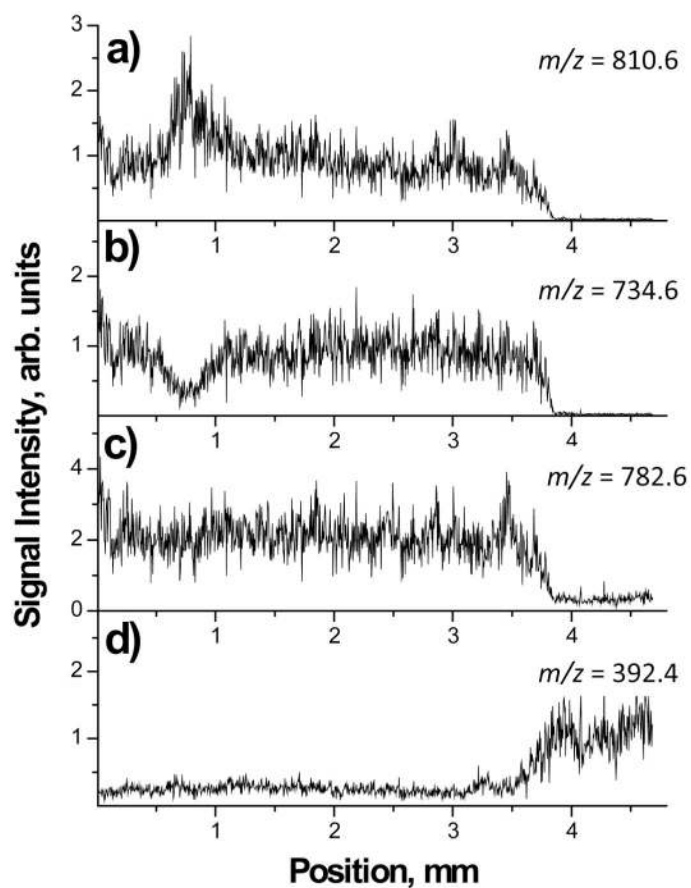
Figure 4.
Representative line profiles of peaks that show a) increase in the white matter (m/z 810.6);
b) decrease in the white matter (m/z 734.6); c) peaks evenly distributed throughout the tissue
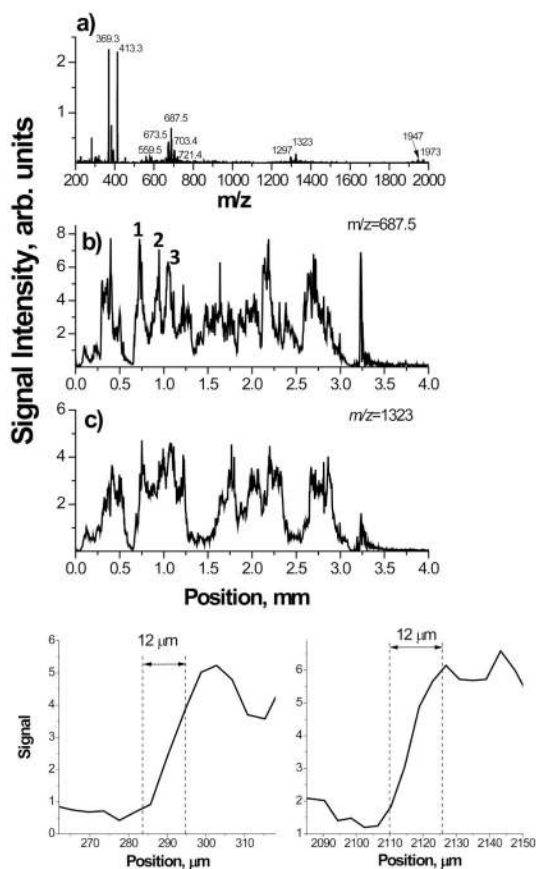sample (m/z 782.6); d) solvent peak (m/z 392.4).

Figure 5.
NanoDESI analysis of papillary renal cell carcinoma (RCC) human tissue sample: a) averaged nanoDESI spectrum. Representative line profiles of the characteristic cholesteryl ester peaks at b) *m/z* 687.5, and c) *m/z* 1323. Numbers in panel b) highlight the features marked in Figure 6. Panels d) and e) show the expanded view of two representative sharp features in the line scan of *m/z* 687.5 demonstrating the increase in the ion signal from ca. 20% to ca. 80% over 12 μm.
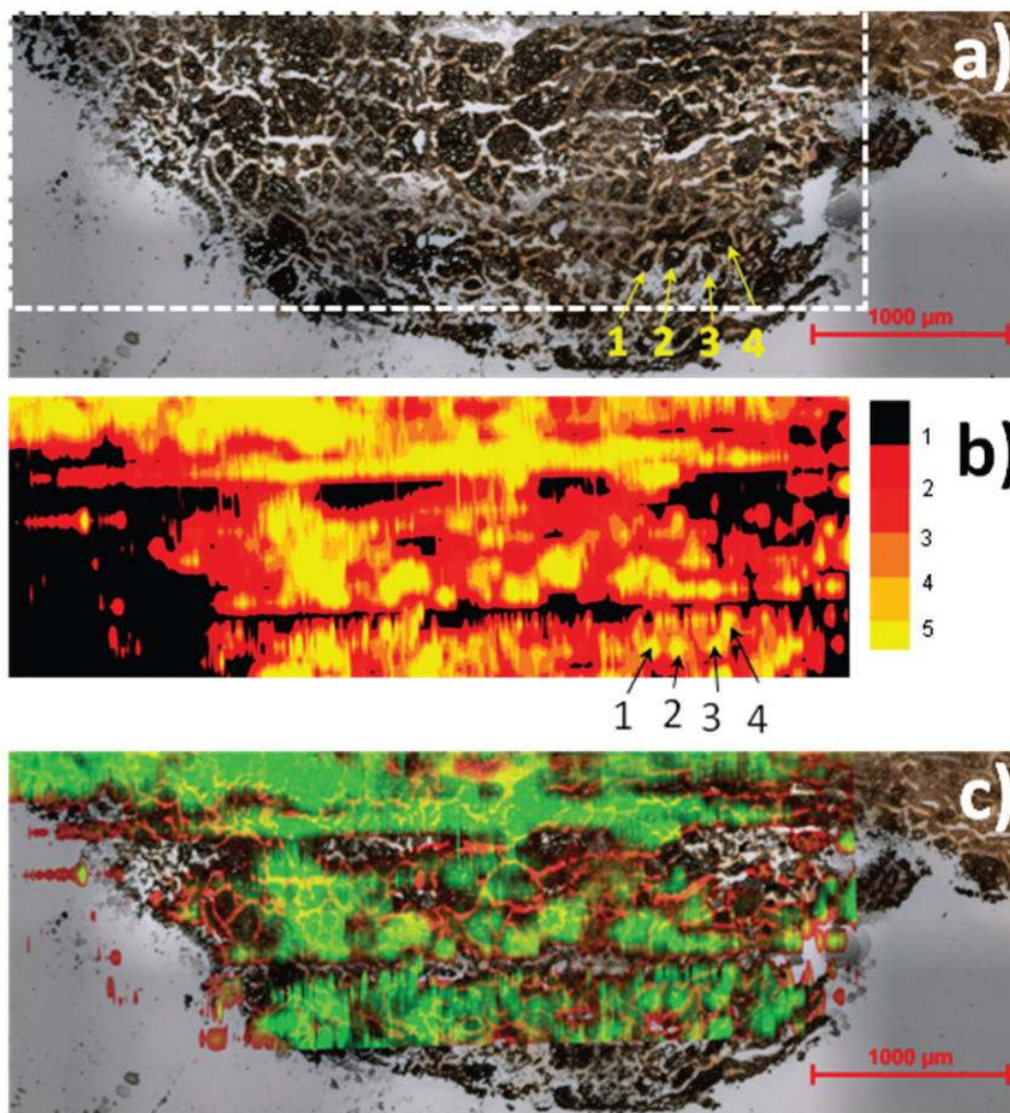
Figure 6.
NanoDESI imaging of a 4.5 mm × 2.5 mm section of the papillary RCC human tissue sample. a) optical image the tissue section; dashed line shows the region analyzed using nano-DESI. b) representative ion image of the cholesteryl ester at *m/z* 687.5; the vertical scale shows the same signal intensity as in Figure 5. c) overlaid optical and ion images. Four small features in the optical image (1,2,3 and 4) are marked in panels a) and b) to facilitate the comparison. Acquisition parameters: 1100 spectra per line in the x-dimension (1 spectrum per 4.1 μm), 100 μm step in the y-dimension. Scale bar = 1000 μm.